Experimental Thermal and Fluid Science 83 (2017) 157–168

Contents lists available at ScienceDirect

Experimental Thermal and Fluid Science

journal homepage: www.elsevier.com/locate/etfs

Effect of channel height and mass flux on highly subcooled horizontal flow boiling

Maria C. Vlachou [a], John S. Lioumbas [a], Kostantinos David [b], Dimitrios Chasapis [b], Thodoris D. Karapantsios [a,*]

[a] Department of Chemistry, Aristotle University of Thessaloniki, University Box 116, 54124 Thessaloniki, Greece
[b] Mechanical Engineering Department, Technical University of Serres, 62124 Serres, Greece

ARTICLE INFO

Article history:
Received 23 September 2016
Received in revised form 18 December 2016
Accepted 3 January 2017
Available online 5 January 2017

Keywords:
Boiling incipience
Aging effect
Heat transfer coefficient
Hydraulic diameter
Flow boiling map
Onset of nucleate boiling

ABSTRACT

Experiments of highly subcooled flow boiling of water in horizontal macrochannels with orthogonal cross-section are performed. Explored parameters are channel height (3 and 10 mm) and mass flux (330–830 kg/m^2 s). The range of applied heat fluxes is 200–1000 kW/m^2. Aging of the copper boiling surface is examined during a 48 h continuous operation and is found to gradually reduce heat transfer rates compared to a polished surface. Yet, aging reaches a steady condition already at 24 h of operation with about 10% lower heat transfer rates than for the polished surface. Using the steady aged surface in the main experiments, three heat transfer regions are identified: (a) forced convection region, before the onset of boiling, depending highly on mass flux but for the most part being channel height independent, (b) nucleate boiling region depending highly on channel height but for the most part being mass flux independent, and (c) a transition region in-between depending on both mass flux and channel height. The 3 mm channel promotes initiation of boiling at lower wall superheats leading to better heat transfer efficiency compared to the 10 mm channel, except for the highest mass fluxes where their performance is comparable. The largest enhancement in heat transfer coefficient provided by the 3 mm channel compared to the 10 mm channel is ~15–20% and is found at the lowest mass flux 330 kg/m^2 s. Analysis of the present data supports the notion that heat transfer is dictated by the thickness of the thermal boundary layer and the density of active nucleation sites.

1. Introduction

Flow boiling has received considerable attention over recent decades because of the high heat fluxes achieved with relatively small increments of the boiling surface temperature and with the compact size of the equipment. Subcooled flow boiling takes advantage of absorbing substantial wall heat fluxes while at the same time the bulk liquid temperature remains below saturation [1]. Subcooling conditions lead vapor bubbles to grow and detach rapidly and then re-condense, when they move from the superheated near wall region (i.e. thermal boundary layer) to the cold bulk liquid [2]. This bubble behavior prevents film boiling and dry-out of the liquid layer, which would occur at high vapor qualities (>0.5) and would decrease heat transfer rates [3]. The advantage of avoiding a net generation of vapor, which may cause problems of pressure rise and vapor agglomeration in the recirculation of closed cooling systems [4], makes the subcooled flow boiling a very efficient and attractive heat removal process. Therefore, it is not surprising that subcooled flow boiling is commonly practiced in heat removal applications that involve large heat dissipation capabilities, such as power production, laser systems and packed electronics [5].

Subcooled boiling region, which is also known as partial boiling or boiling inception, begins with the onset of nucleate boiling (ONB), where the relevant heat transfer mechanism is dominated by two conflicting processes [2,6]:

(a) Macroconvection due to liquid motion: For a constant heat flux, q″, as mass flux, G, increases the thermal boundary layer becomes thinner (affected by fluid's velocity and properties) and ONB is shifted to higher wall superheats, ΔT_{wall}.
(b) Evaporation of the liquid microlayer close to the heated wall: For a constant mass flux, as heat flux increases thermal boundary becomes thicker and ONB is shifted to lower wall superheats. The presence of bubbles in the thermal

* Corresponding author.
E-mail address: karapant@chem.auth.gr (T.D. Karapantsios).

http://dx.doi.org/10.1016/j.expthermflusci.2017.01.001
0894-1777/

Nomenclature

A	heat exchange area, m^2
A_p	parameter defined by Eq. (10)
C	parameter defined by Eq. (12)
C_p	specific heat, J kg^{-1} K^{-1}
D_h	hydraulic diameter, m
f	darcy friction factor, –
G	mass flux, kg m^{-2} s^{-1}
h	heat transfer coefficient, W m^{-2} K^{-1}
k	thermal conductivity, W m^{-1} K^{-1}
L	channel length, m
l_e	entrance length, m
M	molecular weight, kg mol^{-1}
P	pressure, bar
p_r	reduced pressure, – (absolute pressure/critical pressure)
Pr	Prandl number (C_p μ k^{-1}), –
Q	volumetric flow rate, m^3 s^{-1}
q"	heat flux, W m^{-2}
Re	Reynolds number (ρ u D_h μ^{-1}), –
S	parameter defined by Eq. (13)
T	temperature, °C
u	velocity, m s^{-1}
w	channel width, m
x	channel height, m

Greek symbols

α	channel aspect ratio (x/w)
ΔH	latent heat of vaporization, J kg^{-1}
ΔT	temperature difference, °C
Δx	distance, m
μ	dynamic viscosity, N s m^{-2}
ρ	density, kg m^{-3}
σ	surface tension, N m^{-1}
φ	contact angle, °

Subscripts

aver	average
f	film
FC	forced convection
in	inlet
mix	mixing cup
out	outlet
sat	saturation
sub	subcooling
wall	heated wall

boundary layer constitutes the two-phase thermal boundary layer and its thickness is affected also by bubble dynamics (size, velocity).

The influence of the above two mechanisms on flow boiling efficiency is significantly affected by the interplay of the various parameters involved in the process (e.g. channel geometry, surface and fluid properties, operating conditions, degree of subcooling, ΔT_{sub}). As a consequence, the wide diversity of influences of those factors practically rules out a coherent theory that could predict heat and mass transport phenomena during subcooled flow boiling [7,8].

Thus, despite the large number of studies that have experimentally examined the effect of various parameters on flow boiling, none can safely describe the influence of channel's size on heat transfer characteristics (ONB, heat transfer coefficient, h, wall superheat) during subcooled flow boiling. In microchannels (hydraulic diameter, D_h: 10–200 μm), there are works stating that decreasing the channel size increases the heat transfer coefficient [9–12], but there is also evidence for the opposite [13]. This conflict originates from the flow patterns that occur at different combinations of channel size and working conditions (mass and heat flux) affecting the heat transfer mechanism. The conditions that result in bubbles restricted by the limited size of the channel do not allow liquid replenishment to the heated wall and deteriorate heat transfer [11,13]. In minichannels (D_h: 200 μm – 3 mm), the effect is more prevalent, as literature consents that the heat transfer performance improves with the size reduction, because the smaller the size the lower wall superheat and heat flux are needed to initiate boiling. The enhancement caused by size reduction in minichannels is attributed to the larger radial gradient of the liquid axial velocity, which reinforces shear force on nucleated bubbles [14–16]. However, in both mini- and micro- channels it has been found that apart from the channel's diameter/size, the aspect ratio α (height/width), influences heat transfer performance as well, as it could modify the flow patterns because of the change in the cross-section area [17–19].

Conventional size channels (D_h > 3 mm), often referred to as macrochannels, are large enough to permit bubble nucleation, growth and detachment, unlike micro- and mini- channels, where a single bubble can plug the whole cross-sectional area [20]. In all size cases though, microscale phenomena in the thermal boundary layer define the dominant heat transfer mechanisms, i.e., competition between forced convection and nucleate boiling [21]. Experimental works in macrochannels [1,22] provide confirmation of transitions between heat transfer mechanisms, mainly based on temperature analysis of the thermal boundary layer and the heated surface. Subcooled flow boiling in macro-channels has been widely studied in the past two decades, however a comprehensive work examining and explaining the effect of channel size at different flow rates on heat transfer performance is still missing.

The present study examines the influence of the height, x, of a macrochannel having orthogonal cross-section on heat transfer characteristics (ONB, boiling curve, heat transfer coefficient) during subcooled horizontal flow boiling of water for various heat and mass fluxes. The heat transfer area explored in the current work focuses on the flow boiling incipience region, which is related to high heat transfer coefficients and relatively low wall superheats; namely the optimum conditions for highly efficient cooling devices that have not been sufficiently investigated in existing literature [3]. The examined macrochannel heights are large enough to allow bubble growth and detachment within the thermal boundary layer. Under these conditions, high heat flux values are assessed (i.e. q″ > 700 kW/m^2) without the undesired dryout, which would have appeared in mini- and micro- channels at the same mass fluxes [11,23]. The employment of high subcooling conditions (ΔT_{sub} = 70 °C) contributes to the same direction of avoiding dryout [24,25] and is motivated by specific applications that require instant cooling at extreme conditions (i.e. fire incidents) where violent flow of cold liquids is used to maintain walls at low temperature [26]. In addition, it must be stressed that the heated surface itself, its structure and wettability [27] as well as alterations during the boiling process (aging of the surface) [7,13,28,29] have been seen to affect flow boiling heat transfer

performance. Therefore, before quantifying heat transfer results, the aging effect of the heated surface on the heat transfer process is evaluated. Comparison between boiling curves allows identification of the effects, positive or negative, that mass flux and channel size have on the heat transfer performance of macro-channels.

2. Experimental description

2.1. Flow loop and diagnostics

The experimental setup, as presented schematically in Fig. 1a, consists of the boiling test section (Fig. 1b) installed in a flow loop. The working fluid is deionized water with the addition of 400 ppm NaCl to yield a specific electrical conductivity of 100 μS/cm, necessary for void fraction measurement. The employed small amount of NaCl does not affect water physical properties, e.g., boiling point elevation <0.005 °C, but is necessary for the electrical measurement operate of void fraction [30] (see below). Water is stored in a 1.6 m tall orthogonal supply tank (500 L) made of plexiglass®. A progressive cavity pump (Sydex, K-032-1S, 1 hp) is used to circulate water during experiments. A polypropylene cartridge filter (pore size 25 μm) is installed at the discharge line of the pump to prohibit dirt from entering the test section. Flow rate is controlled by an inverter (LS Industrial Systems, Starvert SV-iC5 Frequency Inverter), which adjusts pump's motor speed and by a by-pass line which returns part of the flow stream to the supply tank. Tubing and parts of the flow loop have 1 in inner diameter and are made of PVC at the inlet and stainless steel at the outlet of the test section. The outlet part of the test section is insulated to suppress thermal losses. Outlet is divided in two parallel lines, which are operated individually; a line for void fraction measurement and a line for mixing-cup temperature measurement. The void fraction measurement line is made of polycarbonate transparent tube with two stainless steel ring electrodes flush mounted to

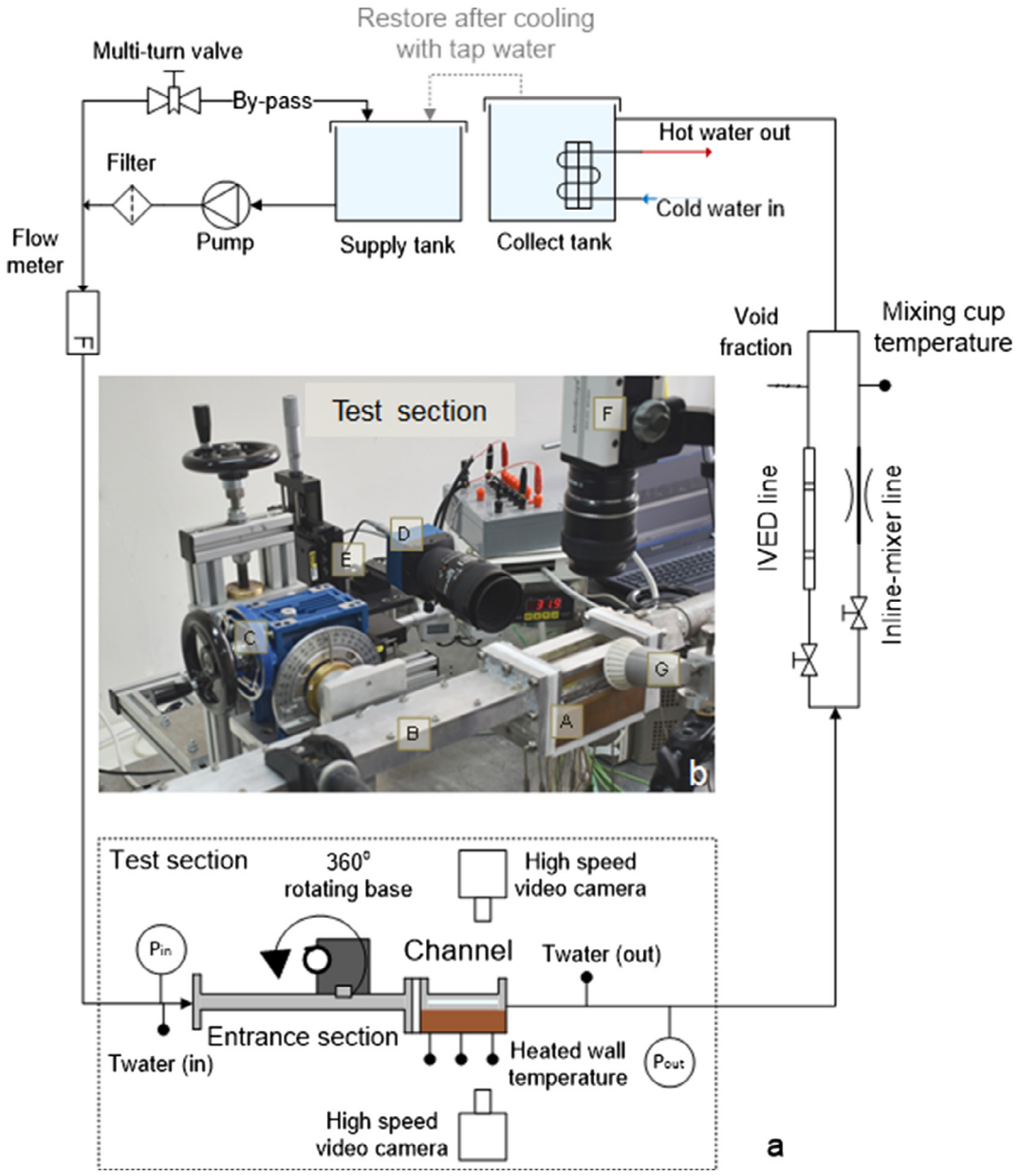

Fig. 1. (a) Schematic diagram of the experimental setup and (b) photograph of the test section. (A) channel, (B) entrance section, (C) 360° rotating base, (D) Side high speed video camera, (E) x-y-z micrometer stage, (F) Top high speed video camera, (G) Led light.

the inner perimeter of the tube and apart by a distance equal to the tube diameter. The mixing-cup temperature measurement line is equipped with an in-line static mixer (Koflo, 1 in – 6 elements). The two-phase flow stream ends up to a collect tank (stainless steel, 500 L) where it is cooled down by tap water flowing in a secondary spiral loop.

Volumetric flow rate is measured by three independent means: (i) a totalizer (CD one-trp, tcm 142/08–4627, accuracy ±2% of measured value) which computes the cumulative volume of flowing water, (ii) two variable area rotameters; one for low flow rates (Kytola C-4C-A, range 1–10 L/min, accuracy ±5% of measured value), one for high flow rates (Kytola D-4E-A, range 10–100 L/min, accuracy ±5% of measured value) which allow observation of the instantaneous flow rate, and (iii) a paddle wheel transmitter (Burkert 8035, range 0.3–10 m/s, accuracy ±2.5% of measured value), which allows continuous recording of the flow rate with respect to time. All flow rate measurement instruments are calibrated against accurate volume/time measurements. The rotameters provide a direct indication of flow stability during runs, while the paddle wheel transmitter allows post processing of the recorded flow history. It turns out that all three flow rate instruments yield similar values of flow rate during the experiments. Pressure is continuously recorded at the inlet, before the entrance section and outlet, just after the exit of the channel by two absolute pressure transducers (Wika S-10, range 0–2.5 bar, accuracy <0.25% of span). A pressure gauge (Wika, EN 837-1, 0–1 bar) is also installed at the inlet of the test section as an indicator, at the same position with the inlet transducer. Void fraction of the two-phase stream at the exit of the test section is measured by an ultrasensitive impedance technique; IVED [30]. In this study, no void fraction data are presented because of the high degree of subcooling, which makes most bubbles to re-condense before reaching the measurement point.

Working fluid and heated wall temperatures are obtained by K-type, ungrounded thermocouples (Uteco, 2 mm, accuracy after calibration ±0.1 °C, response time $t_{0.5}$ = 0.80 s, $t_{0.9}$ = 2.60 s).

2.2. Test section

The test section, as shown in Fig. 1b, includes the heated channel (A) with the corresponding unheated entrance section (B) of the same cross-section.

The entrance section permits the development of the flow before it reaches the heated channel and has different length for the two examined channel heights. Entrance section has a length twice the value calculated from Eq. (1) using the highest employed Reynolds number and turbulent flow (l_e = 250 mm for channel height 3 mm and l_e = 500 mm for channel height 10 mm) [31].

$$\frac{l_e}{D_h} = 4.4 \cdot Re^{1/6} \quad (1)$$

The entrance section is stably adjusted on a 360° rotating base (C), which allows the test section to attain any inclination around a full circle. Inclination is measured by a digital level meter and protractor (InSize 2173–360, accuracy ±0.2° of measured value). At the present work only the horizontal orientation (0.0°) is examined.

The heated channel has an orthogonal cross-sectional area. Its bottom side is composed by a large copper block (heater) whose free top surface acts as the boiling surface. The other three sides are represented by an aluminum frame having a Π shape that is firmly fixed around and above the heater. The aluminum frame accommodates transparent ceramic windows (Schott Robax®) from all three sides to allow optical observations. The channel configuration is schematically presented in Fig. 2a where the heated surface exposed to the flow is denoted (length 120 mm, width 40 mm). Varying the channel height is achieved by fixing around the copper block a different aluminum frame every time, resulting in channel height 3 or 10 mm, with respective aspect ratio, α, 0.075 and 0.25. It should be mentioned that the particular channel dimensions are chosen to resemble those of a space experiment onboard the International Space Station, RUBI [32]. These dimensions are in accordance with pertinent literature [16,33] of macrochannels. Teflon gaskets, 1 cm thick, before and after the channel ensure thermal insulation of the entrance section and the outlet section from the heated channel.

The heater configuration is illustrated in Fig. 2b and c and consists of a copper block with 14 cartridge heaters inserted into drilled holes offering a maximum power of 5.5 kW (cartridges 1–6, 650 W each, are inserted parallel to the heated length whereas cartridges 8–14, 200 W each, are inserted perpendicular to the heated length). The employed cartridge configuration has been selected based on numerical calculations (Supplementary material S1) that showed uniformly heating of the boiling surface.

The temperature of the working fluid is acquired at the inlet (T_{in}), 5 cm before the entrance section and at the outlet (T_{out}), 5 cm downstream of the exit of the channel, by thermocouples protruding at the center of the flow cross section. At the inlet, flow disturbances caused by the thermocouple are smoothed out when the flow travels through the entrance section, which assures a fully developed velocity profile at the subsequent test section. At the outlet, the flow is already disturbed due to the formation of boiling bubbles and has a non-uniform radial temperature profile. Anyway, the measured T_{out} is considered only indicative of the outlet local average temperature and this is just because there is enough turbulent mixing in the flow in all runs. For solving the energy balance, however, the mixing-cup average temperature of the working fluid at the exit of the channel is required. This is measured right after the location of the inline-mixer (T_{mix}). The temperature inside the copper block is measured by thermocouples inserted at 6 positions (Fig. 2b); two are located 10 mm away from the channel inlet (2 mm below the boiling surface), two in the middle of the channel length (one 2 mm and one 12 mm below from the boiling surface (Fig. 2c) and two 10 mm away from the outlet of the channel (2 mm below the boiling surface). The temperature difference between the middle thermocouples is used to determine heat flux values.

Although the heater and the tubing after the test section are insulated, heat losses to the environment are not negligible. Heat losses are estimated from the difference between the heat provided to the water flow, determined by applying Fourier law in the copper block, and the heat generated by cartridge heaters, determined by Joule's law. Single phase heat transfer experiments are conducted for validation of the above. The value of heat losses is found to lie between 5 and 8.5% of the generated heat, for the highest and the lowest mass flux, respectively. An IR camera (Flir, P660) is used to estimate the efficiency of external insulation by providing the temperature distribution at the external surface of the copper block before and after placing insulation.

Two high speed cameras are employed for simultaneous side-view and top-view flow visualizations. The side camera (D) (Mikrotron, Motionblitz, Eosens mini 2, 60 mm macro lens, 5000–8000 fps) is mounted on an x-y-z micrometer stage (E) (Parker Daedal, 4400 series) for accurate positioning and focusing at the desired spot along the flow. The top camera (F) (Redlake, MotionScope PCI Model, 50 mm macro lens, 500–1000 fps) is installed above the test section at a fixed position to provide top-view observations. Proper lighting (SMD Led, GU10 Spotlight, 7W) is provided from the side (G). Synchronization of the two cameras is achieved by using a flash light. Recordings of measured parameters are made with different data acquisition systems (Advantech, Labview, EBS 20M) and computers.

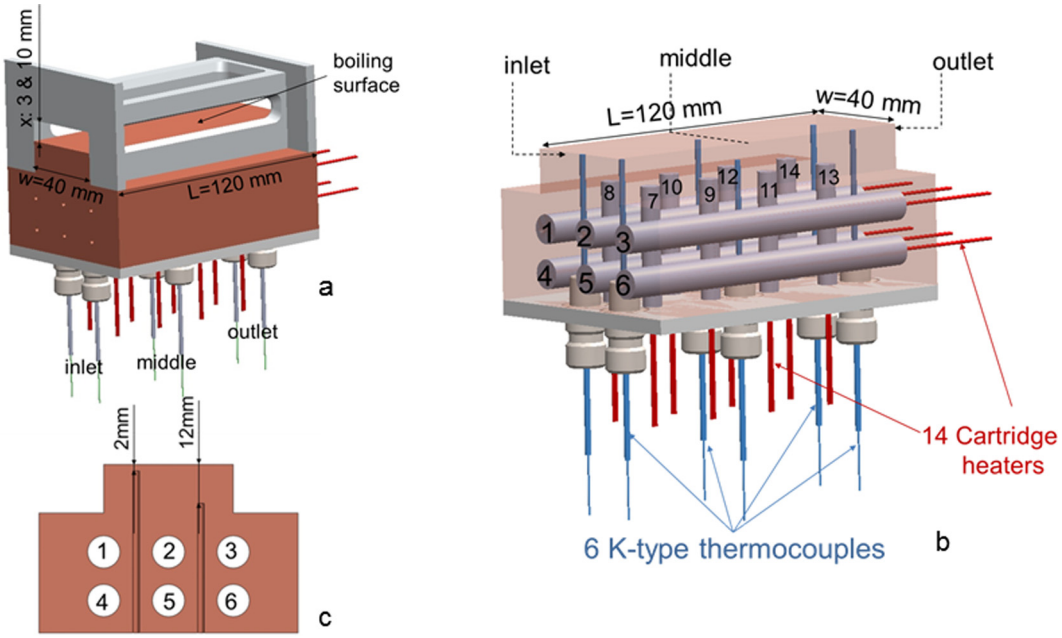

Fig. 2. Schematic diagram of the (a) channel configuration (b) heater configuration and (c) thermocouples location in the middle position.

2.3. Boiling surface

The top, plane, polished surface of the copper block (40×120 mm) is used as the boiling surface (Fig. 3). When fresh and polished, it is fairly hydrophilic (static contact angle: $\varphi = 56 \pm 2°$). After a period of continuous operation (i.e. 3 h) an oxidized layer starts to form on the heated surface, affecting heat transfer performance during time. Changes in both bubble dynamics and heat transfer rates are observed. Aging of the surface reached a steady condition of heat flux and bubble dynamics after 24 h of continuous boiling operation and remained unchanged henceforth (i.e. after 48 h of operation). The color of the heated surface changes due to aging and the surface loses most of its hydrophilic character (static contact angle: $\varphi = 83 \pm 2°$). The static contact angle is measured by the sessile drop method, depositing droplets ($7.5 \cdot 10^{-3}$ ml) on the copper surface.

Aging of the exposed copper surface can occur with or without boiling due to physical changes in the micro-structure. Yet, exposure to high temperatures and boiling conditions, accelerate the process [34]. The effect of aging is examined only in experiments with the 10 mm channel height. Channel height is not expected to have an impact on the oxidation process of the boiling surface; it would only have a slight impact on the time that steady condition is reached due to the different heat flux and wall superheat conditions. The main course of the present flow boiling experimental investigations is held exclusively with steady-aged surfaces (>24 h).

2.4. Experimental procedure

All experiments are conducted at atmospheric pressure. Experiments begin by starting the pump and adjusting the flow rate to the desired value. Next the heater is powered at a certain value. Heat flux is tuned by activating different combinations of cartridge heaters every time (Fig. 2b) and by fine adjustment of the supplied voltage with a variac controller. For every experiment, an initial waiting period of 8 min is allowed to achieve steady state conditions, which are recognized by the heater's minimal temperature variation (±0.1 °C). When steady conditions are reached, continuous recordings of flow rate, temperature, pressure and void fraction are made for a period of 1 min. Within this period, consecutive high speed videos from the two cameras are taken of 1 s duration each. After all data are stored, a new experiment begins by readjusting the flow rate or/and heat flux. At every set of experimental conditions at least three runs are conducted to check for repeatability. Error bars are added to all data markers in the plots representing standard deviation at the specific conditions. Table 1 summarizes the employed working conditions.

2.5. Data reduction

The quantities directly measured are the volumetric flow rate (Q), inlet and outlet pressure (P), temperature inside the heater (T) at several locations, local temperature of the working fluid at the inlet (T_{in}) and outlet (T_{out}) as well as the mixing-cup at the

Fig. 3. Aging effect of the exposed copper boiling surface: oxidation layer changes its color and wettability.

Table 1
Working conditions.

Parameter	Value/range	Unit
Subcooling, ΔT_{sub}	70	°C
Mass fluxes, G	330–830	kg/m^2 s
Heat fluxes, q″	200–1000	kW/m^2
Channel height	3 & 10	mm
Channel width	40	mm
Channel length, L	120	mm

outlet (T_{mix}). Average bulk liquid temperature (T_{aver}) is defined as follows.

$$T_{aver} = \frac{T_{in} + T_{mix}}{2} \tag{2}$$

The temperature differences of subcooling and wall superheat are defined as:

$$\Delta T_{sub} = T_{sat} - T_{in} \tag{3}$$

$$\Delta T_{wall} = T_{wall} - T_{sat} \tag{4}$$

T_{sat} is the saturation temperature at the pressure of the fluid. T_{wall} is calculated by applying the Fourier law of conduction inside the copper block using as inputs the measured temperatures below the heated surface.

The heat flux provided in the test section (q″) is calculated from one dimensional Fourier law of conduction using as inputs the measured temperature difference of the two middle thermocouples that are positioned 10 mm apart from each other in the direction of heat flow (Fig. 2c).

The average flow boiling heat transfer coefficient (h) is calculated by:

$$h = \frac{q''}{T_{wall} - T_{aver}} \tag{5}$$

Reference values for the heat transfer coefficient are calculated for comparison with the experimentally obtained values. In the forced convection region (single phase), h_{FC} is estimated from the correlation of Gnielinski [35], with the friction factor, f, obtained from Moody's diagram for a smooth pipe and with the fluid properties calculated at the film temperature, T_f:

$$T_f = \frac{T_{wall} + T_{aver}}{2} \tag{6}$$

$$h_{FC} = \frac{Nu \cdot k}{D_h} \tag{7}$$

$$Nu = \frac{\frac{f}{8}(Re - 1000) \cdot Pr}{1 + 12.7\left(\frac{f}{8}\right)^{\frac{1}{2}}\left(Pr^{\frac{2}{3}} - 1\right)} \tag{8}$$

Reference values for the heat transfer coefficient in the subcooled flow boiling region, h, are estimated from the correlation of Liu and Winterton [36]:

$$h = \frac{\sqrt{(A_P S \Delta T_{wall})^2 q^{\frac{4}{3}} - q^2}}{\Delta T_{wall}} \cdot q_*^{\frac{3}{2}} \tag{9}$$

where A_P and q^* are obtained from:

$$A_P = 55 \cdot p_r^{0.12}(-\log p_r)^{-0.55} M^{-0.5} \tag{10}$$

$$q_*^3 - C q_*^2 - 1 = 0 \tag{11}$$

$$C = \left(\frac{A_P S}{h_{FC}}\right)^2 \left[\frac{\sqrt{(A_P S \Delta T_{wall})^2 q^{\frac{4}{3}} - q^2}}{\Delta T_{wall}} \cdot (T_{wall} - T_{aver})\right]^{\frac{4}{3}} \tag{12}$$

$$S = \left(1 + 0.055 Re^{0.16}\right)^{-1} \tag{13}$$

p_r is the reduced pressure and M is the molecular weight. Fluid properties in Re are calculated at T_{aver}.

3. Results and discussion

3.1. Aging effect of the boiling surface on flow boiling heat transfer characteristics

The thermal performance of a polished, a 3 h-aged and a 24 h-aged surface is presented in Fig. 4a. Aging tests are conducted for several mass fluxes (330–630 kg/m^2 s) and for a specific initial value of heat flux, which was 540 kW/m^2 for time zero and polished surface, but decreased as boiling proceeds. It is seen that aging leads to deterioration of heat removal, as also mentioned in literature. Several physical phenomena that take place during boiling, such as erosion, corrosion, oxidation, filling of pores and cavities with impurities, etc. have been all reported to decrease heat transfer rates [7,28,29]. More specifically, having the polished surface as reference, the 3 h-aged surface removes 91.5% and the 24 h-aged 90% of the heat flux for the polished surface. In other words, after 24 h of continuous operation a permanent condition is reached at which heat flux removal of the aged surface reduces by 10% compared to the polished and it is steady at further boiling. Beside heat removal, wall temperature varies as well with the aging of the boiling surface, affecting the thickness of the thermal boundary. Fig. 4a shows that for each mass flux (330–630 kg/m^2 s) the wall temperature for the aged surface is lower than for the polished one, therefore with thinner thermal boundary layer over the hot surface.

Aging of the surface changes bubble dynamics on the heated surface, too (Fig. 4b). Despite the fairly hydrophilic nature of the polished surface (Fig 3) many bubbles appear simultaneously on it, covering a large part of it (Supplementary material S2). This is because the high heat flux and high wall temperature yield a high density of active nucleation sites on the surface. Some of the formed bubbles grow large in size while vibrating and wobbling gently around their axis of symmetry without sliding or detachment. There are also bubbles of smaller size that remain unchanged in size and position, simply stuck at their nucleation site. A dynamic balance between evaporation of the liquid microlayer close to the heater wall and re-condensation at the apex of the bubbles exposed to cold liquid may explain the temporary stability of those bubbles. Only a few of them slide in between and sometimes are dragged towards larger bubbles and coalescence. In addition, there is evidence that at high heat fluxes on polished surfaces the vapor recoil effect creates a strong adhesion to the heater that prevents bubble departure which in turn might explain why bubbles resist sliding and detachment [37].

On the other hand, the thermal resistance of the oxidized layer on the 24 h-aged surface hinders heat transfer leading to a lower heat flux and a lower T_{wall}. This yields a much lower density of active nucleation sites and therefore much less simultaneous bubbles (Supplementary material S3). Although the aged surface is less hydrophilic than the polished one, the liquid flow does not allow a stable contact of those sparse bubbles with the solid surface but make them slide along the heated length, detach and recondense in the bulk subcooled flow. In line with our observations, Wang and Dhir [38] also found that active nucleation site density

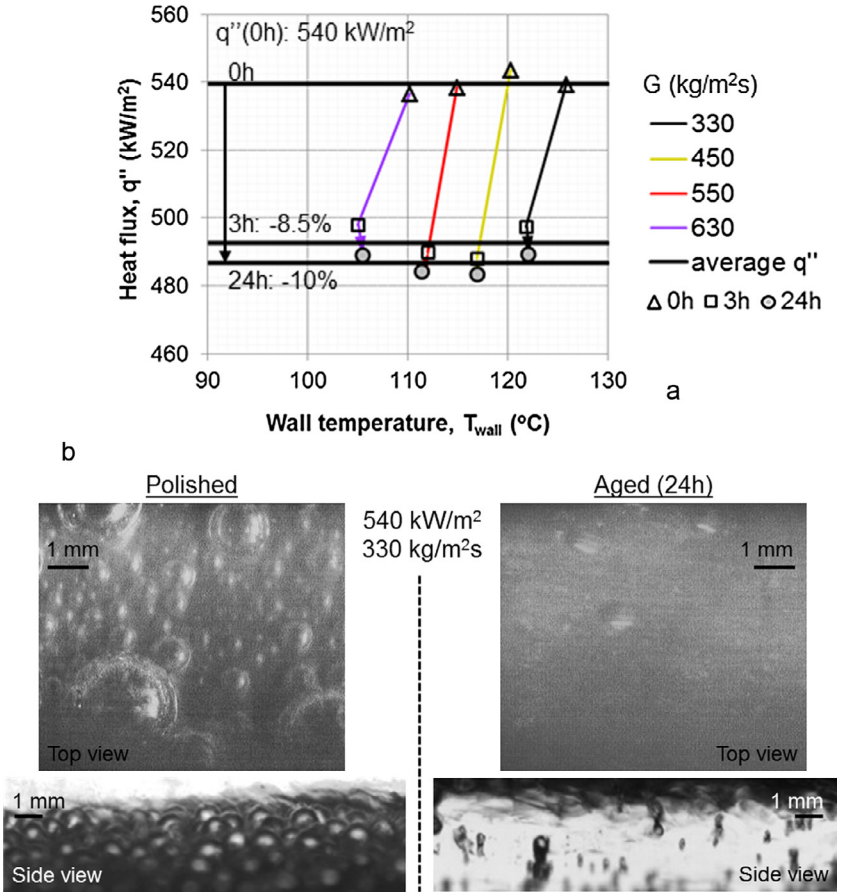

Fig. 4. Surface aging effect on heat transfer characteristics for heat flux 540 kW/m^2 and mass flux 330 kg/m^2 s: (a) heat removal for various mass fluxes; 0 h (△), 3 h (□), 24 h (○) and (b) bubble dynamics.

decreased during oxidation of copper surfaces in water because of the changes in wettability.

3.2. Effect of mass flux on flow boiling heat transfer characteristics

Fig. 5 presents boiling curves for the two channels at various mass fluxes, G. It is apparent that G has a stronger effect on boiling curves in the 10 mm channel; for this reason, a denser matrix of G values is examined. According to literature [21,31], two are the major competing mechanisms in subcooled flow boiling heat transfer. At low heat fluxes, q″, forced convection (FC) dominates, which is the single phase heat transfer mechanism, when only liquid is present without bubble nucleation and wall temperature is below or close to saturation (i.e. $\Delta T_{wall} \sim 0$ °C). At FC, the heat transfer coefficients, h, are affected by both q″ and G (Fig 6) and the thermal boundary layer thickness decreases with increasing G. On the contrary, at high q″ values nucleate boiling (NB) dominates, which is the heat transfer mechanism at which intense boiling occurs and wall temperature is considerably higher than saturation (i.e. $\Delta T_{wall} > 10$ °C). At NB, the effect of G is minimal and only an increasing q″ leads to higher h values (Fig 6). This behavior implies that when NB dominates, the agitation in the thermal boundary layer induced by the formation of bubbles is much more effective than the turbulence mixing induced by forced convection alone. The above are in line with evidence in literature as described at the Introduction [2,6]. Between the forced convection and nucleate boiling regions, a transition region exists, where both mechanisms contribute appreciably to heat transfer [6].

In Fig. 5, as ΔT_{wall} increases from below saturation (negative values) the dominant heat transfer mechanism is forced convection (blue area: single phase region). In this region, an increase in G at a given q″ decreases T_{wall} and thereby delays the onset of boiling (ONB). ONB designates the appearance of first bubbles on the boiling surface as detected from high speed images. ONB is depicted by a thick blue line. Above ONB there is the transition region where mass flux, G, continues to play a measurable role on heat transfer rate. The end of the transition region and the beginning of the NB region is associated with an abrupt increase of the slope in each boiling curve also related with intensification of boiling. This kink point refers to the formation of a bubbly layer within the thermal boundary layer. The graphically determined beginning of NB region is shown as a thick red line. In this region, a further increase in q″ leads to a much higher ΔT_{wall} and activation of so many nucleation sites that the boiling curves become pretty independent of mass flux (red area). The convergence of boiling curves to a somewhat single line could only be detected in the case of the 10 mm channel height and for $\Delta T_{wall} > 40$ °C (Fig. 5b), since only at those tests high enough q″ values are attained.

In Fig. 6, at the FC region h varies with G from 3.9 to 7.3 kW/m^2 K and from 4.2 to 7.5 kW/m^2 K for the small and the large channel, respectively, and at the NB region rise up to 9 kW/m^2 K for both channels. The small inset plots in Fig. 6 show the variation of water outlet temperature (T_{mix}) with q″ for different G values.

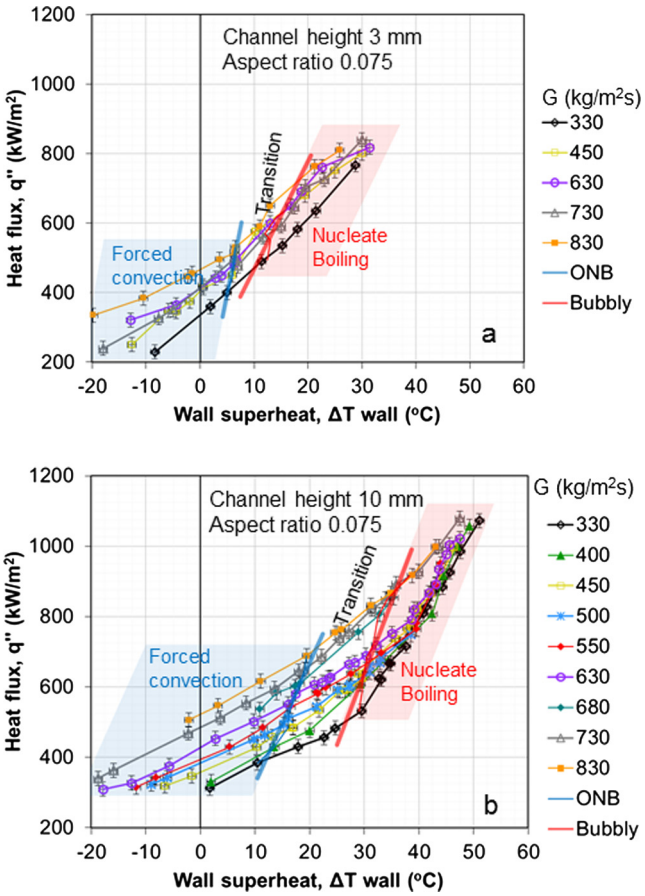

Fig. 5. Effect of mass flux on boiling curves for (a) 3 mm channel height (α: 0.075) and (b) 10 mm channel height (α: 0.25).

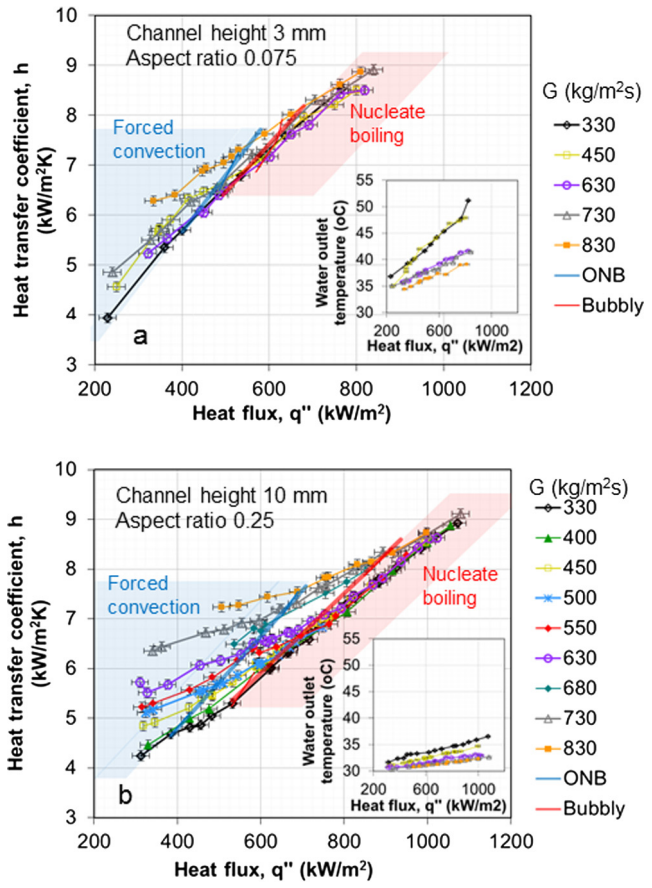

Fig. 6. Effect of mass flux on heat transfer coefficient for (a) 3 mm channel height (α: 0.075) and (b) 10 mm channel height (α: 0.25). Small graphs: effect of mass flux on water outlet temperature.

For the same G value water temperature rise is larger in the small channel. This might be explained if one considers that for the same G value the fluid mass flow rate is much higher in the large channel and it is known that high fluid velocities shift the activation of nucleation sites to higher wall superheats. This is discussed in more detail in Section 3.3 with respect to comparisons between results of the two channels.

Recent works in macro-tubes [39–41] provide experimental confirmation of these transitions between heat transfer mechanisms, mainly based in temperature analysis. Lucic, et al. [22] studied the temperature field in the thermal boundary layer during subcooled flow boiling of water and have shown that the temperature gradient in the thermal boundary layer governs the bubble formation and growth in a rectangular macro-channel (8×10 mm). They measured the thickness of the thermal boundary layer and the temperature field at the phase-interface between fluid and bubble with holographic interferometry at a high temporal and spatial resolution and found that thickness decreases with increasing Reynolds number. This proves the justification of the mass flux effect on the heat transfer mechanisms.

The present experimental h values are compared with h values computed from existing correlations for channels under forced convection in the single-phase region [35] and under flow boiling in the two-phase region [36] (equations described in Section 2.5). The values of the present experimental parameters fall within the range of applicability of these correlations (G, q″, Re, Pr, ΔT_{sub}, ΔT_{wall}). Fig. 7 shows that the two-phase flow boiling model by Liu and Winterton [36] underpredicts the h values of this study. Experimental values lie between −20 and −40% of the predicted ones for both the small and large channel. The inset plots of Fig. 7 compare experimental h values with predicted ones by the model of Gnielinski [35] for convective (single phase) heat transfer and show that they bear the same variation with the flow boiling h values. The deviation between the predictions of the empirical correlations and the current data could be attributed to the one-sided short heating length that is employed in the current experiments and also to the amount of dissolved gas, which is not taken into consideration, as also suggested by Hua, et al. [8].

3.3. Effect of channel height on flow boiling heat transfer characteristics

A comparison of boiling curves between the small and large channel for different G values is provided in Fig. 8. At low G value (Fig 8a) the boiling curve of the small channel is for the most part above the curve of the large channel indicating a better heat transfer efficiency of the small channel. This, however, becomes less evident as G increases, with the two boiling curves approaching each other (Fig 8b). Eventually, for the highest G value (Fig 8c) the boiling curves merge together. Therefore, the effect of channel height on heat transfer varies with mass flux. When G increases the effect of channel height diminishes as a consequence of convective heat transfer domination.

In the forced convection region (single-phase, ΔT_{wall} close to zero) the effect of channel height is minimal for all the examined G values. Yet, for every G the ONB in the small channel occurs at a lower ΔT_{wall} than in the large channel. In addition, ONB in the small channel occurs at lower q″ values except from the case of

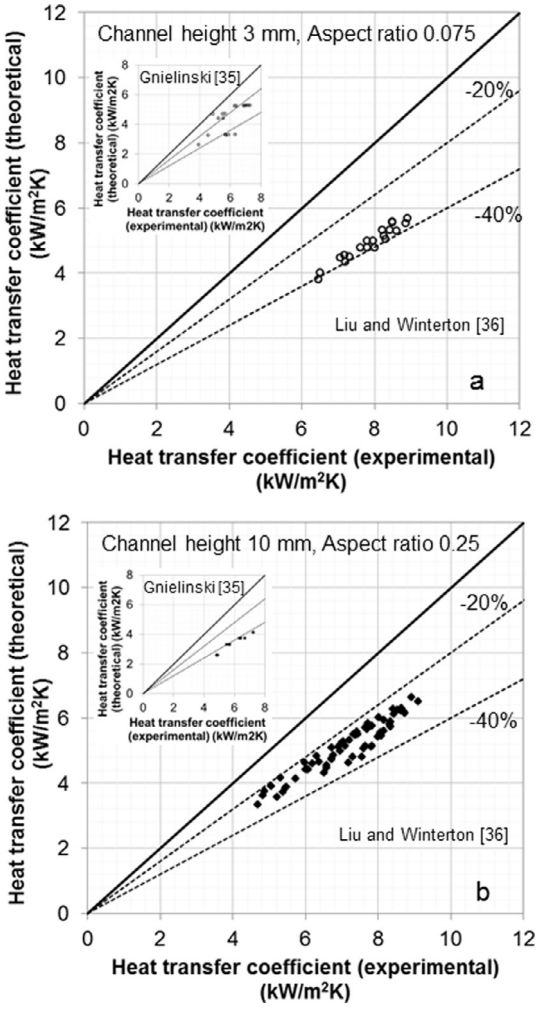

Fig. 7. Comparison between the calculated heat transfer coefficients using correlations and the current experimental values: (a) 3 mm channel height (α: 0.075) and (b) 10 mm channel height (α: 0.25).

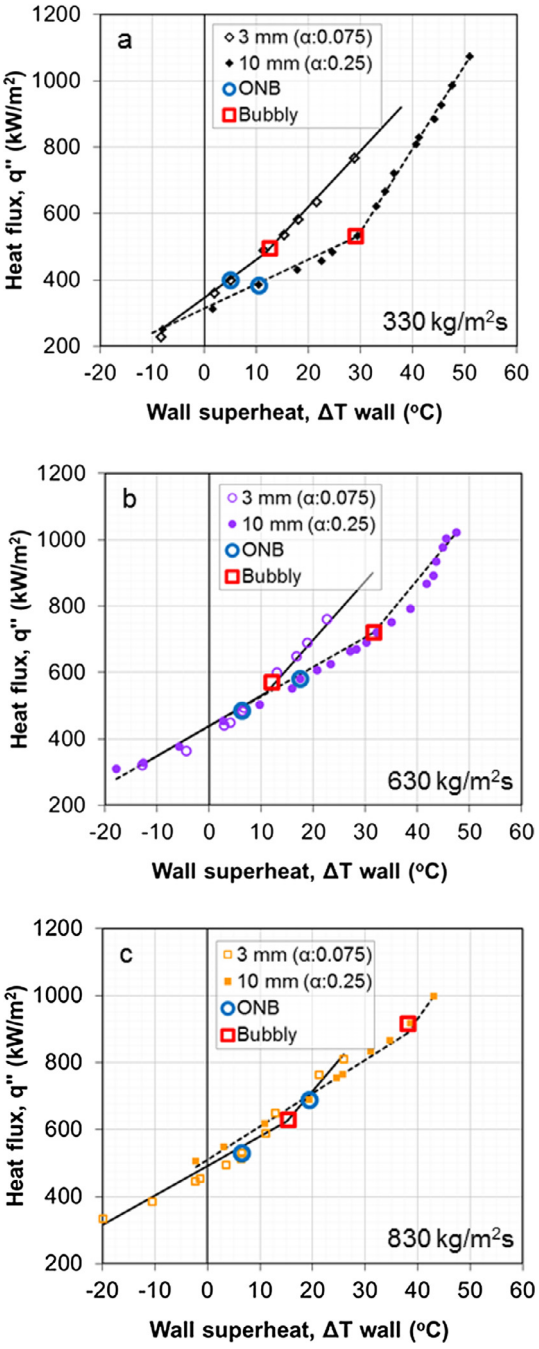

Fig. 8. Effect of channel size on boiling curves for different mass fluxes: (a) 330 kg/m^2 s, (b) 630 kg/m^2 s, (c) 830 kg/m^2 s.

the lowest G (330 kg/m^2 s), where the necessary q″ to initiate boiling is almost the same for the two channels. Similar shifts of the boiling curves with channel size and G were observed by Chen, et al. [15] in mini-channels. Relevant literature [14–16] agrees that heat transfer performance improves with size reduction. It has also been noted that lower wall superheat and imposed heat flux are needed to initiate the boiling on the heated surface for a smaller size and that there are different boiling regimes observed for the same working conditions. In mini- and micro-channels this is a result of the larger aspect ratio, which yields stronger drag forces and enhances bubbles lift-off [18]. Apparently, in macro-channels, where bubbles are not restricted and/or suppressed in channel geometry, the effect of channel height or aspect ratio is the outcome of the interplay between the thermal boundary layer temperature and thickness (it is reminded that for the same G, the liquid velocity is lower in the small channel). Furthermore, the kink point in the boiling curves, designating nucleate boiling (bubbly flow), occurs always at lower ΔT_{wall} and q″ values in the small channel regardless the mass flux value. This, too, manifests a better heat transfer efficiency of the small channel in a sense that nucleate boiling starts to contribute to heat transfer at lower wall superheats.

The effect of decreasing channel height from 10 to 3 mm (α from 0.25 to 0.075) to the heat transfer coefficient, h, is presented collectively in Fig. 9. Positive changes (in percentage) correspond to enhancement in h due to channel height reduction. Heat transfer coefficients are interpolated for different G and q″ values; 400 kW/m^2 (forced convection), 600 kW/m^2 (transition region) and 800 kW/m^2 (nucleate boiling). A detailed table with all values of h for all examined G can be found as Supplementary material (S4). The following can be noted with regards to Fig. 9:

- In the forced convection region, the small channel is more efficient by about 17% only at low G (<500 kg/m^2 s). At higher G values, mass flux effect is very strong and dominates the thermal boundary layer so the large channel becomes more efficient.

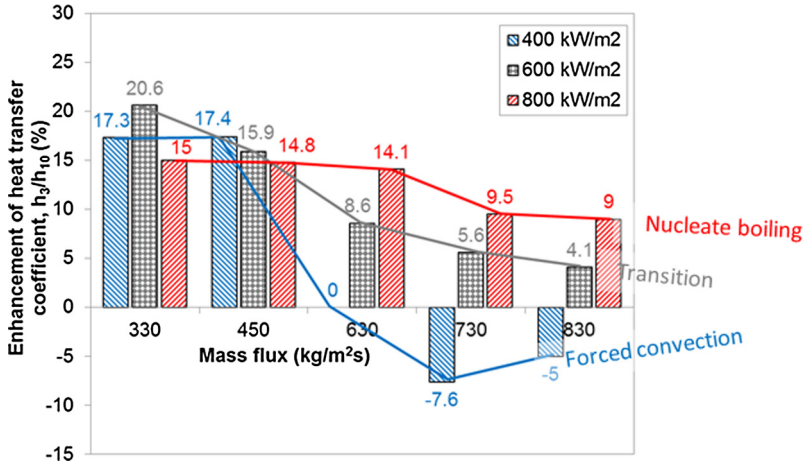

Fig. 9. Percentage of heat transfer coefficient change when decreasing channel height from 10 to 3 mm (aspect ratio from 0.25 to 0.075).

- In the transition region, the small channel is more efficient for all the examined G values: by 20.6% for the lowest G and 4.1% for the highest G. At this region both force convection and nucleate boiling contribute to the heat transfer coefficient.
- In the nucleate boiling region, again the small channel is more efficient for all G values, as in the transition region. At low G (<500 kg/m^2 s) there is a 15% enhancement in h but it drops to 9% at high G.

At first glance, the overall better thermal efficiency of the small channel may look strange because in the small channel lower Reynolds numbers prevail (i.e. Re_{3mm}: 2500–6300, Re_{10mm}: 6800–16,800) which are associated with lower turbulent mixing intensity at the interface between the two-phase thermal boundary layer and the boiling surface. However, one has to consider that although the increased turbulent mixing in the large channel boosts convective heat transfer, by decreasing thermal boundary layer thickness, it also hampers boiling heat transfer, by shifting the activation of nucleation sites to higher wall superheats (Fig. 8). This argument is in agreement with earlier evidence in boiling literature [2,6,22] but it is also a common knowledge that increased fluid velocities shift nucleation phenomena to higher degrees of supersaturation [5]. Consequently, the net effect of these competing phenomena dictates the final heat transfer rates. As depicted in the present experimental results, the incipience of boiling at low ΔT_{wall} and q″ values, makes the small channel more efficient than the large channel except for the very high mass flux where forced convection dominates, Fig. 8c.

3.4. Subcooled flow boiling incipient map

Fig. 10 presents boiling incipient maps for the two channels. The flow boiling incipient map is determined by plotting the flow rate versus the heat flux and demonstrates the regions identified by the boiling curves and the dominant heat transfer mechanisms in previous sections. ONB is determined from high speed images, recognized from the first bubble appearance and depicted at higher q″ as G increases (blue line). Further increase in q″ increases bubble population. Bubbly regime is distinguished by the kink (slope changing) point in boiling curves (red line).

The present experiments at high degree of subcooling (ΔT_{sub} = 70 °C) show clearly the existence of a transition region between the forced convection (single phase) region and the nucleate boiling (two-phase) region. During the transition region, bubble dynamics and thus the heat transfer coefficient are affected

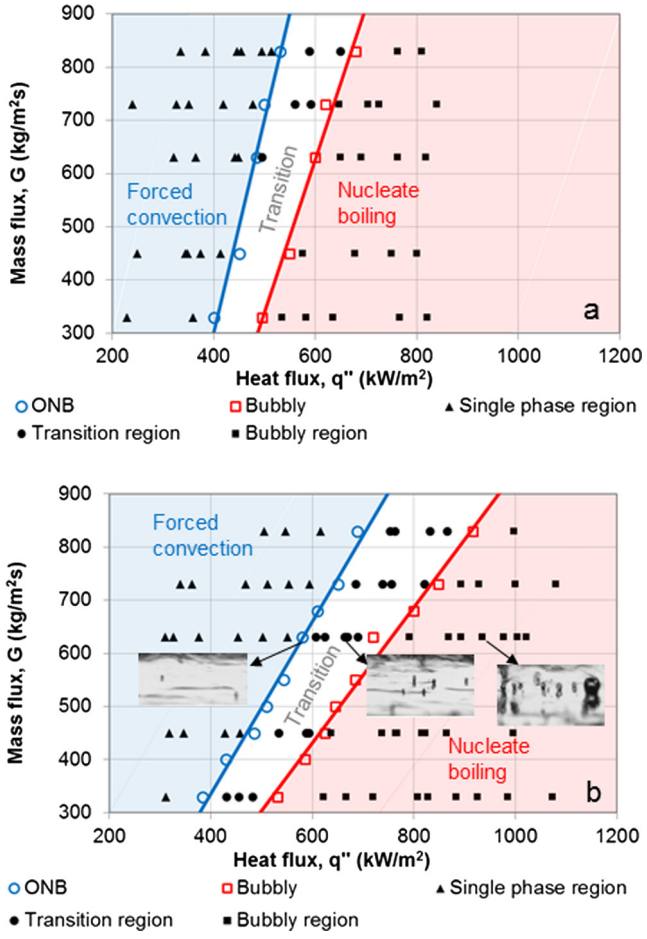

Fig. 10. Flow boiling map for (a) small and (b) large channel.

both by G and x, as already discussed in previous sections. In literature, regions with more dispersed bubbles were found to have better heat transfer performance [42,43] and those regimes are encountered in the examined macro-channels. The transition region for the 3 mm channel height with α = 0.075 is smaller compared to the 10 mm channel (α = 0.25), which is in compliance with the literature [44]. Channels with smaller aspect ratio present different boiling regimes and more suppressed boiling regions.

4. Conclusions

The present study reports subcooled flow boiling experiments in horizontal macrochannels under atmospheric pressure conditions. Working fluid is deionized water at 30 °C inlet temperature. The parameters explored in a broad range of heat fluxes are: aging of the boiling surface, mass flux and channel height. The fresh, polished, copper boiling surface shows better heat transfer performance than the aged surface which is covered by an oxidized layer. At steady aging conditions, after 24 h of operation, this deterioration is 10%. Boiling curves consist of three regions: a forced convection single-phase region before the onset of boiling, a transition region and a nucleate boiling two-phase region. In the forced convection region heat transfer depends on mass flux and not on channel height. In the transition region heat transfer depends on both mass flux and channel height. In the nucleate boiling region heat transfer depends on channel height but not on mass flux. The experimentally determined heat transfer coefficients deviate from predictions of suitable empirical models in literature between −20% and −40% for both the single phase and two-phase regions. The 3 mm height channel has a better thermal efficiency than the 10 mm height channel. This is because nucleate boiling in the small channel is initiated at lower wall superheats compared to the large channel. This is chiefly due to the lower Reynolds numbers, i.e., mass flow rates, in the small channel (for each mass flux) that allow a higher density of active nucleation sites at lower wall superheats. The above outscores the negative effect of a thicker thermal boundary layer at lower fluid velocities. Boiling maps are constructed for both channel heights. These maps mark in a comprehensive way the boundaries between the three heat transfer regions, information which is necessary for the monitoring and improvement of thermal systems and components. An overall evaluation of the examined macrochannels reveals that in order to increase efficiency of boiling applications, the optimum working conditions are small channel and low mass fluxes, preferably in the transition region of boiling.

Acknowledgments

This research was supported by the European Space Agency (Contract No. 4000106405/12/NL/PA on highly efficient flow boiling macrostructured/ macroporous channels) and IKY Fellowships of Excellence for Postgraduate Studies in Greece (the SIEMENS Program). The work was performed under the umbrella of COST Action MP1106. Support of Dr. Christian Schwarz, Technical Officer of ESA (4000106405/12/NL/PA) is also acknowledged.

Appendix A. Supplementary data

Supplementary data associated with this article can be found, in the online version, at http://dx.doi.org/10.1016/j.expthermflusci.2017.01.001.

References

[1] R. Maurus, T. Sattelmayer, Bubble and boundary layer behaviour in subcooled flow boiling, Int. J. Therm. Sci. 45 (3) (2006) 257–268.
[2] H. Steiner, A. Kobor, L. Gebhard, A wall heat transfer model for subcooled boiling flow, Int. J. Heat Mass Transfer 48 (19–20) (2005) 4161–4173.
[3] J.R. Thome, Engineering Data Book, Wolverine Tube, Inc., 2010.
[4] M.C. Paz, M. Conde, E. Suárez, M. Concheiro, On the effect of surface roughness and material on the subcooled flow boiling of water: experimental study and global correlation, Exp. Therm. Fluid Sci. 64 (2015) 114–124.
[5] J.G. Collier, J.R. Thome, Convective Boiling and Condensation, third ed., Clarendon Press, Oxford, 1994.
[6] L.S. Tong, Y.S. Tang, Boiling Heat Transfer And Two-Phase Flow, 2nd ed., Taylor & Francis, Washington, 1997.
[7] C. Paz, M. Conde, J. Porteiro, M. Concheiro, Effect of heating surface morphology on the size of bubbles during the subcooled flow boiling of water at low pressure, Int. J. Heat Mass Transfer 89 (2015) 770–782.
[8] S. Hua, R. Huang, Z. Li, P. Zhou, Experimental study on the heat transfer characteristics of subcooled flow boiling with cast iron heating surface, Appl. Therm. Eng. 77 (2015) 180–191.
[9] I. Mudawar, M. Bowers, Ultra-high critical heat flux (CHF) for subcooled water flow boiling-I: CHF data and parametric effects for small diameter tubes, Int. J. Heat Mass Transfer 42 (1999) 1405–1428, B..
[10] Y. Wang, K. Sefiane, Effects of heat flux, vapour quality, channel hydraulic diameter on flow boiling heat transfer in variable aspect ratio micro-channels using transparent heating, Int. J. Heat Mass Transfer 55 (9–10) (2012) 2235–2243.
[11] A. Kaya, M.R. Özdemir, A. Koşar, High mass flux flow boiling and critical heat flux in microscale, Int. J. Therm. Sci. 65 (2013) 70–78.
[12] A. Khalili Sadaghiani, A. Koşar, Numerical and experimental investigation on the effects of diameter and length on high mass flux subcooled flow boiling in horizontal microtubes, Int. J. Heat Mass Transfer 92 (2016) 824–837.
[13] D. Deng, R. Chen, H. He, J. Feng, Y. Tang, W. Zhou, Effects of heat flux, mass flux and channel size on flow boiling performance of reentrant porous microchannels, Exp. Therm. Fluid Sci. 64 (2015) 13–22.
[14] L.X. Yang, A. Guo, D. Liu, Experimental investigation of subcooled vertical upward flow boiling in a narrow rectangular channel, Exp. Heat Transfer 29 (2) (2014) 221–243.
[15] C.A. Chen, W.R. Chang, K.W. Li, Y.M. Lie, T.F. Lin, Subcooled flow boiling heat transfer of R-407C and associated bubble characteristics in a narrow annular duct, Int. J. Heat Mass Transfer 52 (13–14) (2009) 3147–3158.
[16] M. Piasecka, An investigation into the influence of different parameters on the onset of boiling in minichannels, Arch. Thermodyn. 33 (4) (2013).
[17] S.G. Singh, A. Kulkarni, S.P. Duttagupta, B.P. Puranik, A. Agrawal, Impact of aspect ratio on flow boiling of water in rectangular microchannels, Exp. Therm. Fluid Sci. 33 (1) (2008) 153–160.
[18] U. Soupremanien, S.L. Person, M. Favre-Marinet, Y. Bultel, Influence of the aspect ratio on boiling flows in rectangular mini-channels, Exp. Therm. Fluid Sci. 35 (5) (2011) 797–809.
[19] B. Markal, O. Aydin, M. Avci, Effect of aspect ratio on saturated flow boiling in microchannels, Int. J. Heat Mass Transfer 93 (2016) 130–143.
[20] C.B. Tibiriçá, G. Ribatski, Flow boiling phenomenological differences between micro- and macroscale channels, Heat Transfer Eng. 36 (11) (2015) 937–942.
[21] G.P. Celata, M. Cumo, A. Mariani, The effect of the tube diameter on the critical heat flux in subcooled flow boiling, Int. J. Heat Mass Transfer 39 (8) (1996) 1755–1757.
[22] A. Lucic, M. Emans, F. Mayinger, C. Zenger, Interferometric and numerical study of the temperature field in the boundary layer and heat transfer in subcooled flow boiling, Int. J. Heat Fluid Flow 25 (2) (2004) 180–195.
[23] L. Cheng, Critical heat flux in microscale channels and confined spaces: a review on experimental studies and prediction methods, Russ. J. Gen. Chem. 82 (12) (2013) 2116–2131.
[24] C.R. Kharangate, L.E. O'Neill, I. Mudawar, M.M. Hasan, H.K. Nahra, R. Balasubramaniam, N.R. Hall, A.M. Macner, J.R. Mackey, Effects of subcooling and two-phase inlet on flow boiling heat transfer and critical heat flux in a horizontal channel with one-sided and double-sided heating, Int. J. Heat Mass Transfer 91 (2015) 1187–1205.
[25] D.-W. Yuan, L.-M. Pan, D. Chen, H. Zhang, J.-H. Wei, Y.-P. Huang, Bubble behavior of high subcooling flow boiling at different system pressure in vertical narrow channel, Appl. Therm. Eng. 31 (16) (2011) 3512–3520.
[26] C.L. Vandervort, A.E. Bergles, M.K. Jensen, An experimental study of critical heat flux in very high heat flux subcooled boiling, Int. J. Heat Mass Transfer 37 (1) (1994) 161–173.
[27] M.C. Vlachou, J.S. Lioumbas, T.D. Karapantsios, Heat transfer enhancement in boiling over modified surfaces: a critical review, Interfacial Phenom. Heat Transfer 3 (4) (2015) 341–367.
[28] C.Y. Lee, B.J. Zhang, K.J. Kim, Morphological change of plain and nano-porous surfaces during boiling and its effect on nucleate pool boiling heat transfer, Exp. Therm. Fluid Sci. 40 (2012) 150–158.
[29] C.S. Sujith Kumar, S. Suresh, C.R. Aneesh, M.C. Santhosh Kumar, A.S. Praveen, K. Raji, Flow boiling heat transfer enhancement on copper surface using Fe doped Al2O3–TiO2 composite coatings, Appl. Surf. Sci. 334 (2015) 102–109.
[30] T.D. Karapantsios, S.P. Evgenidis, K. Zacharias, T. Mesimeris, Method for the detection and characterization of bubbles in liquids and device therefor, Resp. System A1 (2015), 3005942.
[31] F. Kreith, R.M. Manglik, M.S. Bohn, Principles of Heat Transfer, Cengage Learning Inc., USA, 2011.
[32] B. Tóth, E.s.s.M.P. Development, Operations teams, S. Teams, S. Industry, Future experiments to measure liquid-gas phase change and heat transfer phenomena on the International Space Station, Microgravity Sci. Technol. 24 (3) (2011) 189–194.
[33] S.G. Kandlikar, M.J. Howell, Investigation of nuclation and heat transfer for subcooled boiling on microfin surfaces, in: G.P. Celata, P. DiMarco, A. Mariani (Eds.), 2nd European Thermal-Sciences and 14th UIT National Heat Transfer Conference, Edizioni ETS, Rome, 1996, pp. 241–247.
[34] M. Moliere, Y. Verdier, C. Leymonie, Oxidation of copper in high purity water at 70 °C: application to electric generator operation, Corros. Sci. 30 (2–3) (1990) 183–188.
[35] V. Gnielinski, New equations for heat and mass transfer in turbulent pipe and channel flow, Int. Chem. Eng. 16 (2) (1976) 359–368.

[36] Z. Liu, E.H.S. Winterton, A general correlation for saturated and subcooled flow boiling in tubes and annuli, based on a nucleate pool boiling equation, Int. J. Heat Mass Transfer 32 (11) (1991) 2759–2766.
[37] K. Sefiane, D. Benielli, A. Steinchen, A new mechanism for pool boiling crisis, recoil instability and contact angle influence, Colloid Surf. A 142 (2–3) (1998) 361–373.
[38] C.H. Wang, V.K. Dhir, On the gas entrapment and nucleation site density during pool boiling of saturated water, ASME J. Heat Transfer 115 (1993) 670–679.
[39] K. Hata, Y. Shirai, S. Masuzaki, Heat transfer and critical heat flux of subcooled water flow boiling in a horizontal circular tube, Exp Therm Fluid Sci 44 (2013) 844–857.
[40] J. Yan, Q. Bi, Z. Liu, G. Zhu, L. Cai, Subcooled flow boiling heat transfer of water in a circular tube under high heat fluxes and high mass fluxes, Fusion Eng. Des. 100 (2015) 406–418.
[41] J. Yan, Q. Bi, G. Zhu, L. Cai, Q. Yuan, H. Lv, Critical heat flux of highly subcooled water flow boiling in circular tubes with and without internal twisted tapes under high mass fluxes, Int. J. Heat Mass Transfer 95 (2016) 606–619.
[42] T. Harirchian, S.V. Garimella, A comprehensive flow regime map for microchannel flow boiling with quantitative transition criteria, Int. J. Heat Mass Transfer 53 (13–14) (2010) 2694–2702.
[43] S.G. Singh, A. Jain, A. Sridharan, S.P. Duttagupta, A. Agrawal, Flow map and measurement of void fraction and heat transfer coefficient using an image analysis technique for flow boiling of water in a silicon microchannel, J. Micromech. Microeng. 19 (7) (2009) 075004.
[44] T. Harirchian, S.V. Garimella, Effects of channel dimension, heat flux, and mass flux on flow boiling regimes in microchannels, Int. J. Multiphase Flow 35 (4) (2009) 349–362.